AD_____

Award Number: W81XWH-04-01-0697

TITLE: Alpha-v Integrin Targeted PET Imaging of Breast Cancer Angiogenesis and Low-Dose Metronomic Anti-Angiogenic Chemotherapy Efficacy

PRINCIPAL INVESTIGATOR: Xiaoyuan Chen, Ph.D.

CONTRACTING ORGANIZATION: Stanford University School of Medicine
                                              Stanford, CA 94305

REPORT DATE: August 2007

TYPE OF REPORT: Final

PREPARED FOR: U.S. Army Medical Research and Materiel Command
            Fort Detrick, Maryland 21702-5012

DISTRIBUTION STATEMENT: Approved for Public Release;
                                          Distribution Unlimited

The views, opinions and/or findings contained in this report are those of the author(s) and should not be construed as an official Department of the Army position, policy or decision unless so designated by other documentation.

REPORT DOCUMENTATION PAGE

Form Approved
OMB No. 0704-0188

1. REPORT DATE (DD-MM-YYYY)	2. REPORT TYPE	3. DATES COVERED (From - To)
01-08-2007	Final	15 JUL 2004 - 14 JUL 2007

4. TITLE AND SUBTITLE

Alpha-v Integrin Targeted PET Imaging of Breast Cancer Angiogenesis and Low-Dose Metronomic Anti-Angiogenic Chemotherapy Efficacy

5a. CONTRACT NUMBER

5b. GRANT NUMBER
W81XWH-04-01-0697

5c. PROGRAM ELEMENT NUMBER

6. AUTHOR(S)
Xiaoyuan Chen, Ph.D.

E-Mail: shawchen@stanford.edu

5d. PROJECT NUMBER

5e. TASK NUMBER

5f. WORK UNIT NUMBER

7. PERFORMING ORGANIZATION NAME(S) AND ADDRESS(ES)

Stanford University School of Medicine
Stanford, CA 94305

8. PERFORMING ORGANIZATION REPORT NUMBER

9. SPONSORING / MONITORING AGENCY NAME(S) AND ADDRESS(ES)
U.S. Army Medical Research and Materiel Command
Fort Detrick, Maryland 21702-5012

10. SPONSOR/MONITOR'S ACRONYM(S)

11. SPONSOR/MONITOR'S REPORT NUMBER(S)

12. DISTRIBUTION / AVAILABILITY STATEMENT
Approved for Public Release; Distribution Unlimited

13. SUPPLEMENTARY NOTES

14. ABSTRACT
The overall objective of this project is to develop 18F-labeled RGD peptide derivatives for breast cancer imaging with prolonged tumor retention and improved in vivo kinetics to visualize and quantify αv-integrin expression and subsequently evaluate the metronomic anti-angiogenic chemotherapy efficacy on tumor regression, necrosis, and angiogenesis. Specific Aims: (1) To optimize 18F-labeled RGD peptide tracer for breast cancer imaging with prolonged tumor retention and improved in vivo kinetics. (2) To demonstrate the feasibility of PET/18F-RGD to image breast tumor growth, spread, and angiogenesis as well as quantifying αv-integrin expression level during breast tumor neovascularization over time. (3) To evaluate the efficacy of EMD 121974/paclitaxel combination on tumor regression, necrosis, and angiogenesis and demonstrate the feasibility of PET/18F-RGD to monitor the treatment outcomes. Major findings: We have developed a series of novel multimeric RGD peptides for PET imaging. We have also successfully demonstrated that suitably labeled RGD peptide allows quantification of integrin expression in vivo in a non-invasive manner. We have also synthesized a RGD-paclitaxel conjugate for breast cancer integrin targeted therapy.

15. SUBJECT TERMS
No subject terms provided.

16. SECURITY CLASSIFICATION OF:

a. REPORT	b. ABSTRACT	c. THIS PAGE	17. LIMITATION OF ABSTRACT	18. NUMBER OF PAGES	19a. NAME OF RESPONSIBLE PERSON USAMRMC
U	U	U	UU	21	19b. TELEPHONE NUMBER (include area code)

Standard Form 298 (Rev. 8-98)
Prescribed by ANSI Std. Z39.18

Table of Contents

INTRODUCTION

Breast cancer is the most common form of cancer in women. Despite vigorous efforts to diagnose, treat and prevent this disease, it remains a leading cause of death among women. In order to develop new approaches to the treatment of this disease, further knowledge is needed of the basic biology underlying the etiology and progression of the disease. Recent studies have shown that vascularization is significantly higher in node-positive breast tumors than in node-negative tumors, and that a high degree of vascularization is generally associated with a poorer prognosis. This finding has led to the conclusion that inhibition of angiogenesis offers a possible therapeutic modality for a subset of patients. Cell adhesion molecule integrin $\alpha v \beta 3$ plays a pivotal role in tumor angiogenesis and metastasis. The inhibition of integrin activity has been associated with decreased tumor growth in breast cancer xenografts. Synergy of cylic RGD peptide EMD 121974 with radioimmunotherapy (RIT) has resulted in increased efficacy of therapy in a murine breast cancer model.

The purpose of this proposal is to use high-resolution microPET technology to image breast cancer angiogenesis and anti-angiogenic therapy efficacy. The specific aims of the proposed work are as follows:

Specific Aim 1: To optimize ^{18}F-labeled RGD peptide tracers for breast cancer imaging with prolonged tumor retention and improved in vivo kinetics.

Specific Aim 2: To demonstrate the feasibility of PET/^{18}F-RGD to image breast tumor growth, spread and angiogenesis as well as quantifying integrin expression level during breast tumor neovascularization over time.

Specific Aim 3: To evaluate the efficacy of EMD 121974/paclitaxel combination on tumor regression, necrosis and angiogenesis and demonstrate the feasibility of PET/^{18}F-RGD to monitor the treatment outcomes.

This final report will summarize the major achievements based on the originally proposed studies and further discoveries that derived from this DOD BCRP Idea funding mechanism.

BODY

Part I: Development of ^{18}F-labeled RGD peptides for tumor imaging

During the last few years we have developed a series of RGD peptides with high affinity and specificity for integrin αvβ3. With the RGD/integrin system, polyvalency has been shown to be able to significantly improve integrin-binding affinity and selectivity. We used 2 types of assays to examine the interaction between RGD multimers (Fig. 1) and αvβ3 integrin. We first used a cell adhesion assay to assess the antiadhesion effect of RGD multimers against integrin αvβ3. RGD octamer showed significantly better inhibition ability than the monomer/dimer/tetramer counterparts, as could be attributed to the multiple binding sites or significantly increased local concentration. We then performed a cell-binding assay, an often-used method to determine the receptor-binding affinity of a given ligand. Again, the integrin αvβ3-binding affinity followed the order of RGD octamer > RGD tetramer > RGD dimer > RGD monomer (Table 1).
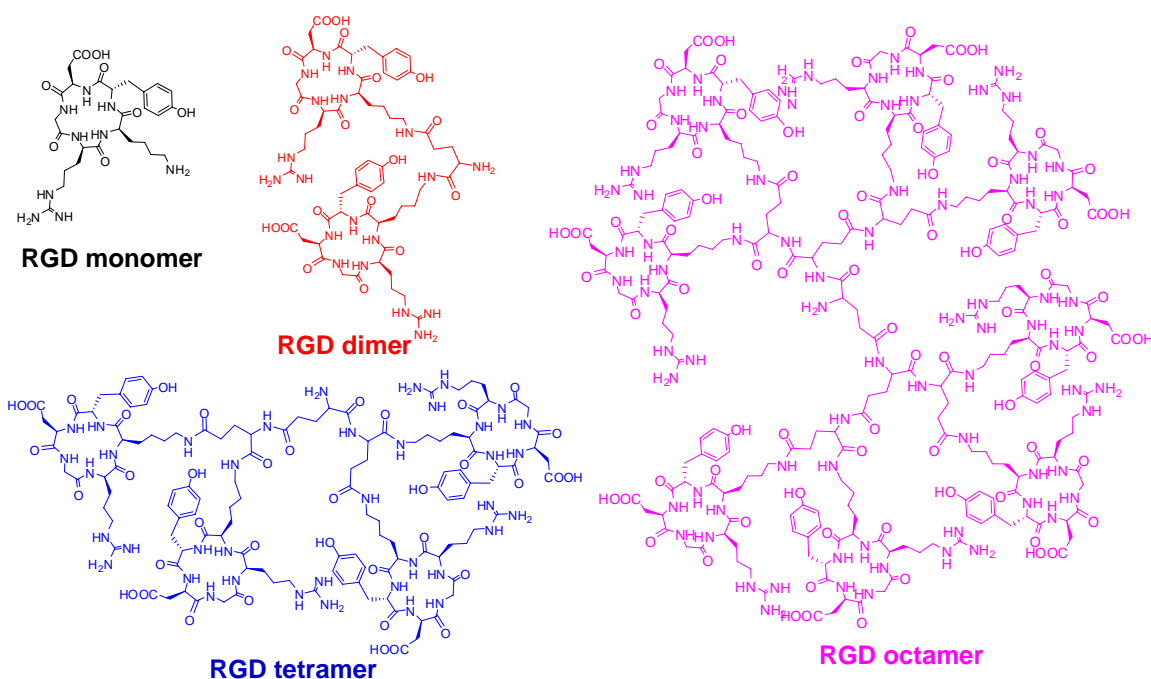

Fig. 1. Schematic structures of c(RGDyK) (RGD monomer), E[c(RGDyK)]2 (RGD dimer), E{E[c(RGDyK)]2}2 (RGD tetramer), and E{E{E[c(RGDyK)]2}2}2 (RGD octamer).

When the RGD peptides were labeled with positron emitting radionuclide ^{64}Cu for positron emission tomography (PET) imaging of tumor integrin expression in vivo, the tumor uptake also showed the pattern of octamer > tetramer > dimer > monomer. However, high molecular weight RGD multimers also had significantly higher background signal and activity accumulation in the kidneys. In particular, the uptake of ^{64}Cu-DOTA-RGD octamer in the kidney was high and persistent, with no appreciable activity excreted to the urinary bladder over time. Such a phenomenon suggests that

receptor-mediated binding might be involved. Indeed, immunohistochemical staining showed that mouse kidneys have high β3 expression on the endothelial cells of small glomerulus vessels. These results indicate that the receptor affinity/specificity, overall molecular charge, hydrophilicity, and molecular size have profound effect on the yumor targeting efficacy and in vivo kinetics. In the case of RGD peptides we feel that RGD dimer or tetramer may be most suitable for ^{18}F-labeling and PET imaging studies.

Table 1. Multivalent enhancement (MVE) of RGD multimers based on cell adhesion and cell binding assays using human glioblastoma U87MG cells. Concentrations are expressed as mean $\pm$ SD (n = 3) and MVE is the IC_{50} values of the RGD monomer divided by the IC_{50} of the RGD multimers.

	RGD monomer	RGD dimer	RGD tetramer	RGD octamer
anti-adhesion IC_{50} (nmol/L)	2710 ± 720	695 ± 99	323 ± 85	106 ± 22
anti-adhesion MVE	1	3.9	8.4	25.6
cell binding IC_{50} (nmol/L)	203 ± 32	103 ± 14	34.6 ± 2.6	10.0 ± 1.7
cell binding MVE	1	1.97	5.87	20.3

We have thus tried to label RGD monomer, dimer, and tetramer with ^{18}F through N-succinimidyl-4-^{18}F-fluorobenzoate (^{18}F-SFB) prosthetic group. The monomeric RGD peptide based tracers have fast blood clearance accompanied by relatively low tumor uptake and rapid tumor washout, presumably due to the suboptimal receptor-binding affinity/selectivity and inadequate contact with the binding pocket located in the extracellular segment of integrin αvβ3. The dimeric RGD peptide tracer ^{18}F-FRGD2 had a significantly higher tumor uptake and prolonged tumor retention compared with ^{18}F-FRGD because of the synergistic effect of bivalency and improved pharmacokinetics (20,32). However, the labeling yield of ^{18}F-FRGD2 was not satisfactory, due in part to the bulk of the 2 cyclic pentapeptides and the prosthetic group ^{18}F-SFB. The glutamate α-amine group has a pKa of 9.47, which is also less reactive than the ε-amino group on the lysine side chain (pKa = 8.95) usually used for ^{18}F labeling of peptides.

PEGylation has been widely used for improving the in vivo kinetics of various pharmaceuticals. We have previously demonstrated that PEGylation of RGD peptides does improve the pharmacokinetics of the resulting tracers. However, insertion of a long PEG also reduced the receptor binding affinity to some extent. In this project, we incorporated a mini-PEG spacer, 11-amino-3,6,9-trioxaundecanoic acid, with three ethylene oxide units, onto the glutamate α-amino group of the dimeric RGD peptide E[c(RGDyK)]₂ (denoted as RGD2). The hypothesis was that the mini-PEG will increase the overall hydrophilicity and alleviate the steric hindrance, thereby increasing the ^{18}F labeling yield. Since the spacer is quite short, such modification is not expected to significantly affect the receptor binding affinity or the in vivo kinetics of the tracer. The mini-PEG spacered dimeric RGD peptide was labeled with ^{18}F through ^{18}F-SFB and evaluated in murine tumor models by microPET imaging.

Comparison of the PET imaging results for ^{18}F-FPRGD2 and ^{18}F-FRGD2 revealed that ^{18}F-FPRGD2 had comparable tumor uptake and non-specific muscle uptake, while the kidney uptake was appreciably lower. The residence time for kidneys (calculated on the basis of the serial PET imaging data) was 0.016 h and 0.029 h for ^{18}F-FPRGD2 and ^{18}F-FRGD2, respectively. The shorter residence time is desirable as the kidney is the only organ with appreciable tracer uptake and is clearly the dose-limiting organ. The uptake of ^{18}F-FPRGD2 in the other major organs (e.g., liver and intestine) is at a very low level (less than 1.5%ID/g at 1 h p.i.) and will unlikely cause any adverse effects. Acute toxicity study of FPRGD2 in Sprague-Dawley rats is currently underway and an exploratory investigational new drug (eIND) application will be filed once the GLP toxicity study is completed.

Part II: PET quantification of tumor integrin expression

In order to assess whether ^{18}F-labeled RGD peptide allows quantification of integrin expression in vivo, we performed dynamic microPET scans in six tumor models (U87MG, MDA-MB-435, PC-3, NCI-H1975, PC-3, and C6). Selected coronal images at different time points postinjection (p.i.) of [^{18}F]FRGD2 in a U87MG tumor mouse were shown in **Fig. 2**. High tumor activity accumulation was observed as early as 5 min p.i. Most of the radioactivity in non-target tissues were cleared at 70 min p.i. The uptakes in the U87MG tumor, kidneys, liver and lung were 3.81 ± 0.80, 2.25 ± 0.43, 1.10 ± 0.22, and 0.59 ± 0.18 %ID/g, respectively. Time-activity curves showed that this tracer excreted predominantly through the renal route (**Fig. 3**A). Diversified tumor uptake patterns of [^{18}F]FRGD2 were found in different xenograft models (**Fig. 3**B). The U87MG tumor had the highest tumor tissue integrin and tumor cell integrin levels and also had highest initial tumor uptake but also had the most rapid tumor washout, reaching a plateau after 50 min p.i. The tumors with low magnitude of tumor uptake had minimal tumor washout, providing reasonably high tumor contrast at late time points when non-specific activity accumulation in the normal organs had been mostly cleared.
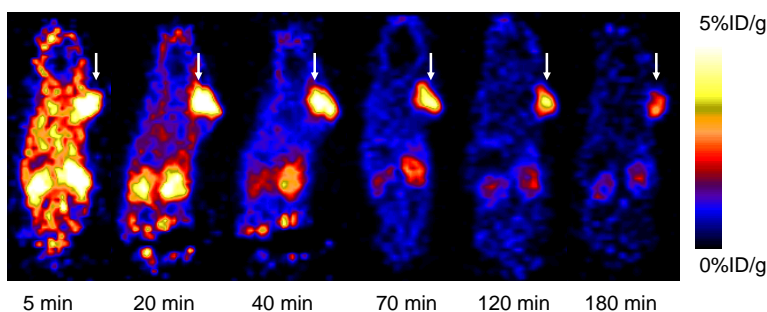

Fig. 2. Dynamic microPET study of U87MG tumor bearing mouse over 60 min after injection of [^{18}F]FRGD2 (100 μCi), static scans at 2 h and 3 h time points were also conducted to complete the tracer kinetic study. Decay-corrected whole-body coronal images that contain the tumor were shown.
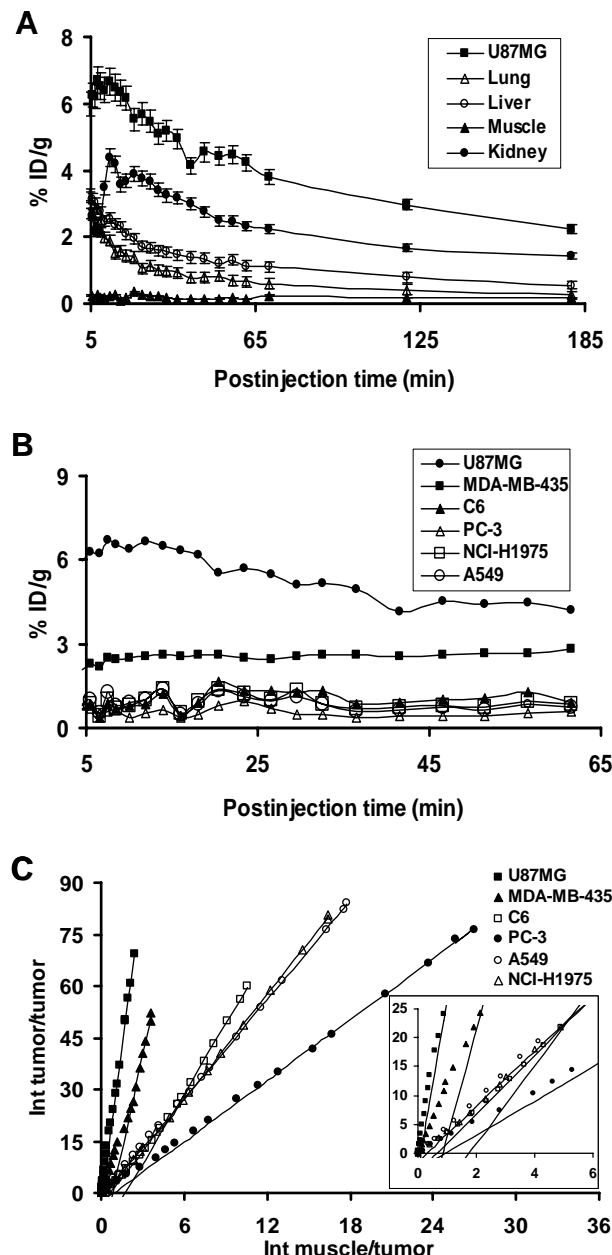
Fig. 3. (A) Time activity curves derived from the 60 min dynamic and 70 min, 120 min, 180 min static microPET imaging study. The regions of interests (ROIs) are shown as mean % ID/g ± SD (n = 3). (B) Comparison of tumor uptake in nude mice derived from the 60 min dynamic microPET scans. (C) Logan plots derived from 60 min dynamic microPET imaging data, which showed excellent linearity of normalized integrated (Int) tumor activity versus normalized integrated muscle tissue activity effective for t > 25 min. The slopes of the fits represent the distribution volume ratios (DVR).

Logan plot is a graphical method of analysis, applicable to ligands that bind reversibly to receptors or enzymes. This method can calculate the DV for dynamic PET data before steady state is actually reached. We used 26.5 min as starting point for linear regression of the dynamic microPET studies since all graphs became linear after that point with the

slope being DVR (**Fig. 3**C). The calculated binding potentials (B_{max}/K_d) for [^{18}F]FRGD2 in the U87MG, MDA-MB-435, C6, PC-3, NCI-H1975, and A549 tumors using muscle as reference tissue were found to be 29.5, 17.5, 5.8, 1.9, 4.1 and 3.8, respectively.

A linear relationship was found between the BP values calculated from graphical analysis of dynamic microPET imaging and the B_{max} values measured from SDS-PAGE/autoradiograms (R^2 = 0.96, P = 0.005) (**Fig. 4**A). The tumor to contralateral background ratios did not provide the same level of correlation with the tumor tissue integrin density at early time points (e.g. Pearson's correlation coefficient R^2 was 0.86 at 5 min and 0.88 at 30 min p.i.) (**Fig. 4**C and D). At 1 h p.i., a good linear relationship was found between tumor/background ratio and tumor integrin level (**Fig. 4**E). Interestingly, tumor cell integrin level did not have the same level of correlation with tumor contrast or binding potential (**Fig. 4**B and F).
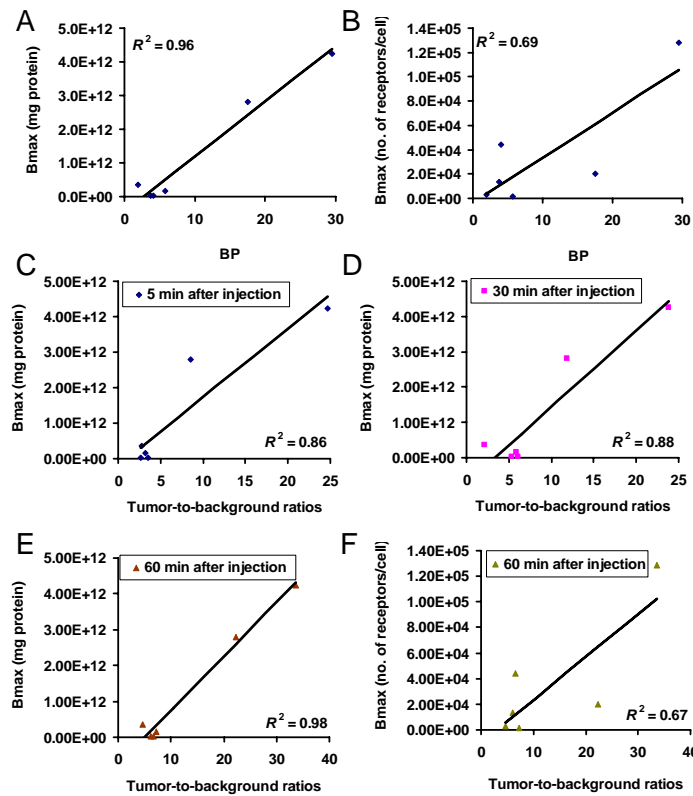

Fig. 4. Correlation analysis between: (A) tumor tissue receptor density vs. binding potential (BP) (calculated from Logan plot transformation of dynamic microPET imaging data) (R^2 = 0.96); (B) tumor cell integrin expression vs. BP (R^2 = 0.69); (C-E) tumor tissue receptor density vs. tumor/background ratios. The coefficient of determination R^2 is about 0.86, 0.87, and 0.98 at 5 min, 30 min, and 60 min postinjection of [^{18}F]FRGD2, respectively; (F) tumor cell receptor density vs. tumor/background ratio at 60 min postinjection of [^{18}F]FRGD2. The coefficient of determination R^2 is 0.67. Data derived from six tumor models (U87MG, C6, MDA-MB-435, PC-3, NCI-H1975, and A549) illustrated excellent linear relationship between tumor tissue receptor density vs. binding potential, and tumor tissue receptor density vs. tumor/background ratio at 1 h p.i..

Part III: In Vivo Treatment Efficacy of RGD-PTX

Targeting drugs to receptors involved in tumor angiogenesis has been demonstrated as a novel and promising approach to improve cancer treatment. In this study, we evaluated the antitumor efficacy of a RGD peptide paclitaxel conjugate (RGD2-PTX) in an orthotopic MDA-MB-435 breast cancer model. Because the dimeric RGD peptide selectively binds to integrin αvβ3 receptors that are overexpressed in both the breast cancer cells and the tumor vasculature, the RGD2-PTX conjugate would specifically accumulate in the integrin positive sites and induce apoptosis or necrosis, resulting in enhanced antitumor activity over PTX. By comparing the biodistribution of [3H]-PTX (Table 2) and [3H]-RGD2-PTX (Table 3), we found that [3H]-RGD2-PTX had higher initial tumor exposure dose and prolonged tumor retention than [3H]-PTX.

Table 2. Tissue distribution of [3H]PTX in Balb/c nude mice bearing MDA-MB-435 tumor. Values are mean ± SD (n=3) and shown as [3H]PTX concentration (ng/g Tissue).

Organ	4h	24h	48h
Blood	67.1±9.8	42.7±14.7	35.0±1.5
Skin	135.1±23.5	24.6±3.2	25.4±9.3
Muscle	257.3±32.2	41.1±17.2	35.4±10.7
Heart	200.7±48.5	37.2±10.7	42.9±10.9
Lung	329.2±18.2	35.2±5.4	47.9±8.8
Liver	2389.3±408.8	123.4±12.2	132.6±31.9
Kidney	339.6±67.6	38.0±13.3	35.7±2.0
Spleen	365.5±118.5	51.6±7.6	36.4±8.4
Stomach	180.7±15.7	24.4±4.7	17.2±4.0
Intestine	274.1±110.1	14.4±2.5	12.8±7.0
tumor	239.0±56.2	85.6±15.2	45.8±1.7
tumor/muscle	0.93	2.08	1.29
tumor/liver	0.1	0.69	0.34
tumor/kidney	0.7	2.25	1.28

Table 3. Tissue distribution of [^{3}H]PTX-RGD in Balb/c nude mice bearing MDA-MB-435 tumor. Values are mean ± SD (n=3) and shown as [^{3}H]PTX-RGD concentration (ng/g Tissue).

Organ	4h	24h	48h
Blood	101.7±30.8	143.1±18.0	225.4±12.8
Skin	144.1±15.9	87.2±16.1	66.0±9.1
Muscle	125.1±24.0	81.2±11.4	85.6±28.0
Heart	228.7±29.8	170.7±18.6	222.5±16.2
Lung	300.4±30.9	238.6±75.6	207.8±48.2
Liver	1252.9±109.9	510.4±28.9	545.3±30.6
Kidney	1421.6±289.8	338.9±22.1	281.8±32.6
Spleen	322.3±59.3	228.7±39.4	227.9±28.2
Stomach	119.0±16.7	71.63±9.5	71.7±12.2
Intestine	127.8±20.3	52.1±7.5	50.8±9.5
tumor	357.5±62.6	229.4±50.4	148.8±40.2
tumor/muscle	2.86	2.82	1.74
tumor/liver	0.29	0.45	0.27
tumor/kidney	0.25	0.68	0.53

To determine whether RGD2-PTX conjugate has better antitumor effect than the combination of PTX+RGD2 (in equal PTX dose) in vivo as we proposed, female athymic nude mice bearing MDA-MB-435 tumor were randomly divided into three groups and treated with vehicle (Saline with 10% DMSO), RGD2 (15 mg/kg) plus PTX (10 mg/kg), or RGD2-PTX conjugate 25 mg/kg (equimolar dose of PTX) every three days (a total of 5 doses). As shown in Fig. 5A, the combination of RGD2 plus PTX therapy started to show significant therapeutic effect as compared with the vehicle control group at day 15 when the treatment was initiated ($P < 0.05$). However, the effectiveness of RGD2-PTX conjugate treatment became obvious as compared to the other two treatments after two doses. After day 9, RGD2-PTX conjugate group showed even more tumor suppression effect ($P < 0.01$ compared with vehicle group, $p < 0.05$ compared with PTX+RGD2 group). Moreover, no significant body weight difference was observed among these three treatment groups (Fig. 5B).
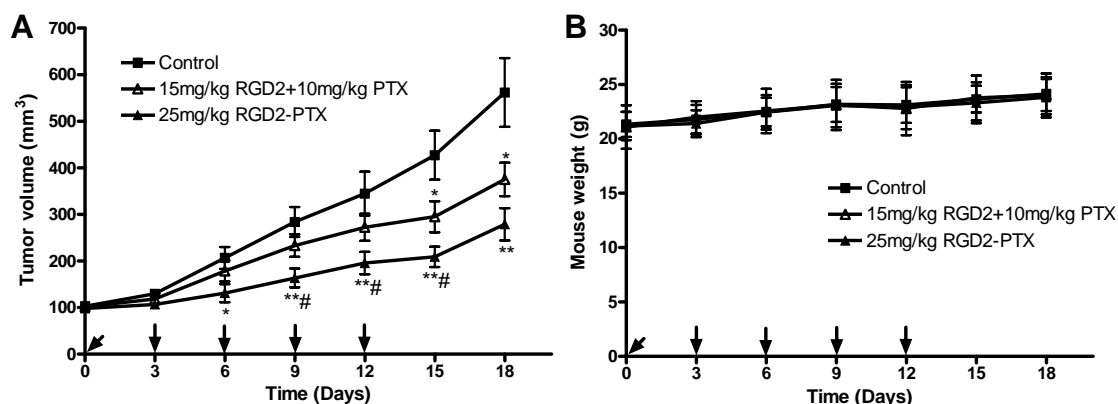
Fig. 5. (A) Effect of solvent only, RGD2+PTX and RGD2-PTX treatment on the growth of MDA-MB-435 breast cancer model. Averaged tumor size was monitored every three days and shown as mean ± SE (n = 8/group). (B) The mice weight of control group or treatment group over time (n = 8/group). The drug administration intervals were indicated by arrows. Where * or # denotes $P < 0.05$, ** denotes $P < 0.01$. * and **, compared with solvent control group, # compared with RGD2+PTX treatment group.

^{18}F-FDG microPET is a functional imaging technique that reflects the glycolytic rate of tissues and has been used to measure the increased metabolic demand in tumor cells. Therefore, we performed ^{18}F-FDG microPET on day 10 after 3 doses of treatment. As shown in Fig. 6, the tumor uptake of ^{18}F-FDG was decreased from 7.95 ± 0.39 %ID/g (vehicle control group) to 6.73 ± 0.50 %ID/g in PTX+RGD2 treatment group, and to 5.97 ± 0.54 %ID/g in RGD2-PTX treatment group ($P < 0.01$). These tumor uptakes during the treatment correlated well with our therapy results at later time points. To assess the effects of therapy on tumor proliferation, ^{18}F-FLT imaging was also conducted. No significant difference was observed among the control and two treatment groups ($P > 0.05$). In fact, the tumor growth curve showed a steady increase of tumor growth in all three groups, which may also suggest that the PTX could not effectively inhibit cell proliferation in this experiment.
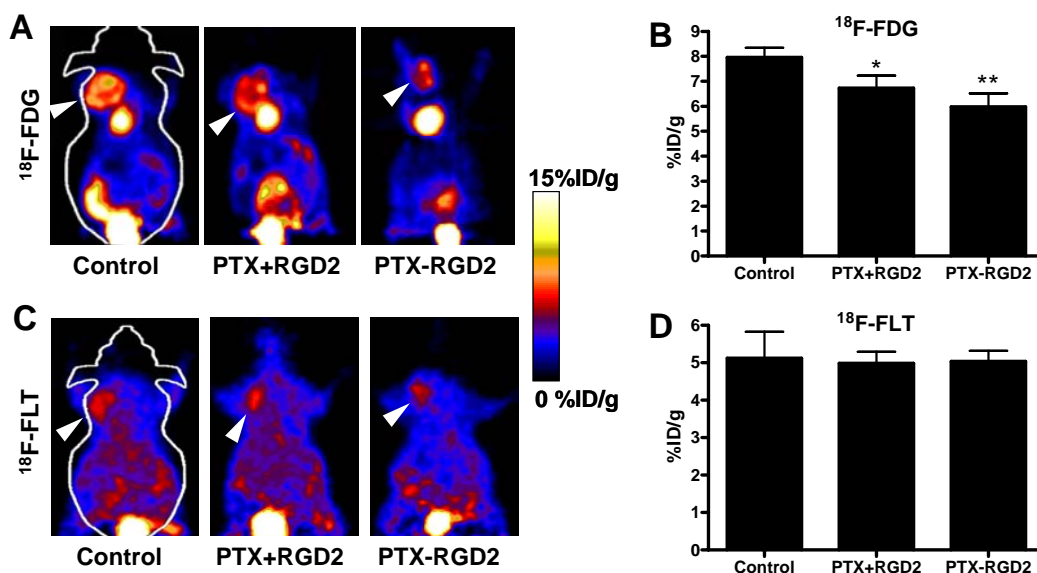
Fig. 6. (A) Representative whole-body coronal microPET images of MDA-MB-435 tumor bearing mice with ^{18}F-FDG at day 10 during the therapy. (B) Comparison between the uptake of ^{18}F-FDG in MDA-MB-435 tumor with solvent treatment only, RGD2+PTX or RGD2-PTX. Regions of interest (ROIs) were shown as %ID/g ± SD (n = 3/group). (C) Representative whole-body coronal microPET images of MDA-MB-435 tumors bearing mice with ^{18}F-FLT at day 11 during the therapy. (D) Comparison between the uptake of ^{18}F-FLT in MDA-MB-435 tumors with solvent treatment only, RGD2+PTX or RGD2-PTX. Regions of interest (ROIs) were shown as %ID/g ± SD (n = 3/group). Tumors were indicated by arrows. Where * denotes P < 0.05, ** denotes P < 0.01.

To evaluate whether cell apoptosis was involved in the RGD2-PTX enhanced regression on MDA-MB-435 tumors, the TUNEL assay was used to quantify cell apoptosis in tumor sections from all three groups. As shown in Fig. 7, vehicle-treated tumors did not show specific cell apoptosis. Combination of RGD2 with PTX for the treatment only resulted in moderately positive TUNEL staining at tumor peripheral area. In contrast, RGD2-PTX conjugate treatment group showed significant cell apoptosis throughout the tumor. At the same time, we also detected human integrin $\alpha_v\beta_3$ expression on the same tissue section by immunofluorescence staining. Although TUNEL staining was quite different among these three groups, all tumor sections showed similar integrin $\alpha_v\beta_3$ expression pattern. For the PTX+RGD2 treatment group, PTX seems to be accumulated only on the angiogenic edge of the tumor and cause apoptosis at the corresponding tumor periphery. The center of the tumor with necrosis and low vessel density does not allow efficient diffusion of PTX and thus little or no PTX induced apoptosis was observed. For the RGD2-PTX treatment group, TUNEL positive staining was found throughout the tumor with excellent overlay with integrin $\alpha_v\beta_3$, confirming the effectiveness of integrin specific delivery of PTX.
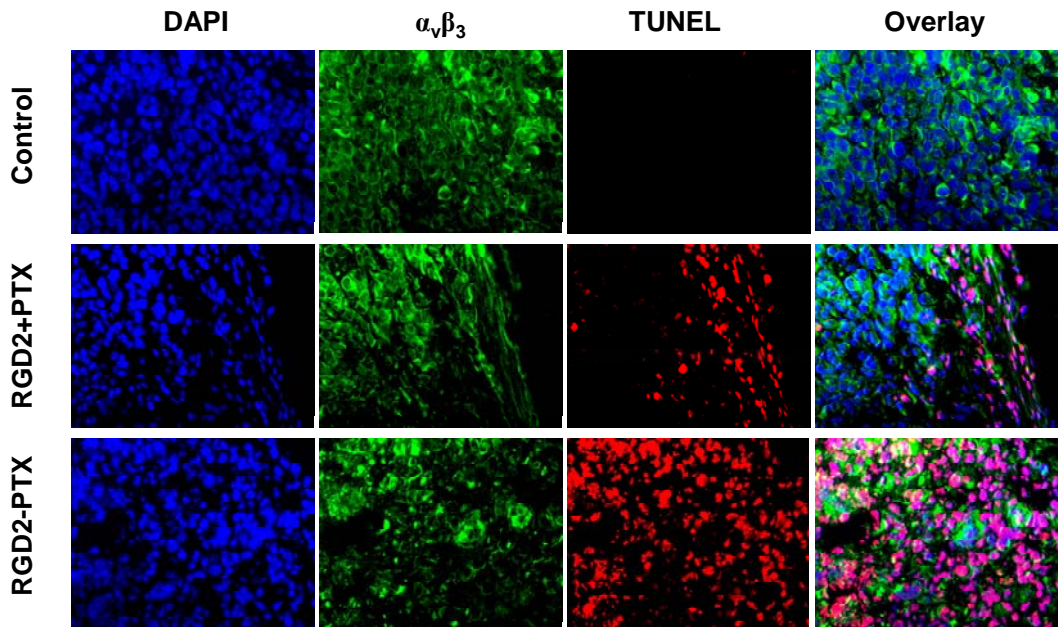

Fig. 7. Immunofluorescence staining of DAPI, human integrin αvβ3, TUNEL and the overlay for MDA-MB-435 tumor tissue from three treatment groups.

We also carried out the CD31 staining to study the effect of PTX treatment on vascular damage. Microvessel density (MVD) analysis revealed that RGD2-PTX treated tumor had significantly lower vessel density (13.3 ± 5.7 vessels/mm^2) than the PTX+RGD2 treated tumor (24.0 ± 3.2 vessels/mm^2; $P < 0.01$) and solvent treated tumor (37.0 ± 8.1 vessels/mm^2; $P < 0.01$). The tumor vessels in PTX+RGD2 treatment group tend to have large diameters while the vessels in the RGD2-PTX treatment group tend to be small and irregular (Fig. 8). To value whether tumor cell proliferation inhibition was also involved in the RGD2-PTX enhanced regression on MDA-MB-435 tumors, the Ki67 (cell proliferation marker) immunofluorescence was used to quantify cell proliferation in tumor sections from all groups. However, no significantly delayed cell proliferation was observed in RGD2-PTX conjugate therapy group compared with vehicle control group and combination (RGD2+PTX) group (Fig. 9), which was also consistent with the ^{18}F-FLT imaging result (Fig. 6).
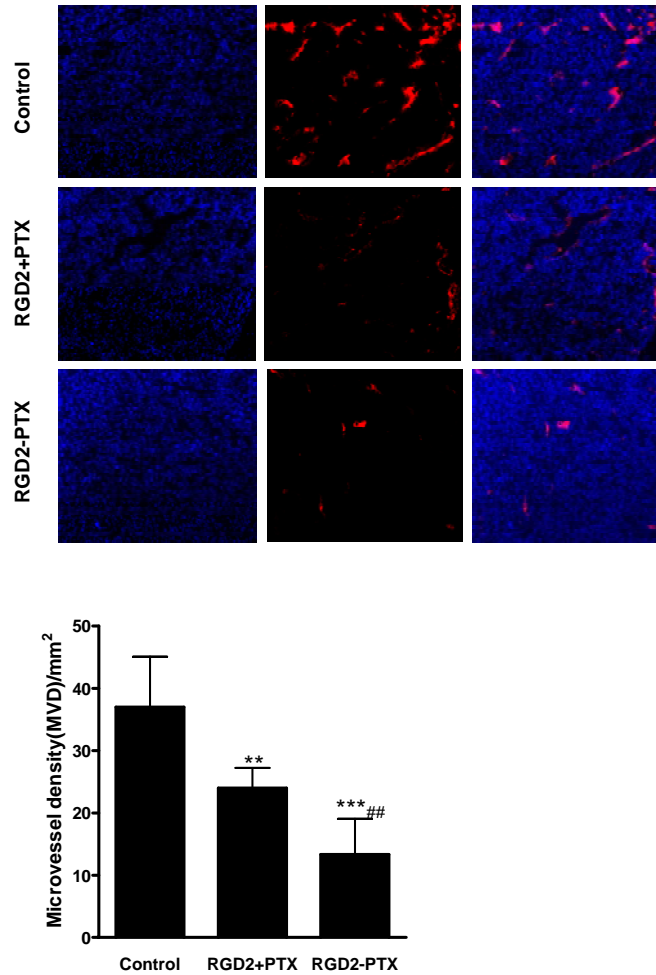

Fig. 8. (A) Immunofluorescence staining of DAPI, CD31, and the overlay for MDA-MB-435 tumor tissues from three treatment groups. (B) Microvessel density (MVD) analysis of MDA-MB-435 tumor tissues from three treatment groups (n = 10/group). Where ** or ## denotes $P < 0.01$, *** denotes $P < 0.01$. ** and ***, compared with solvent control group, ## compared with RGD2+PTX treatment group.
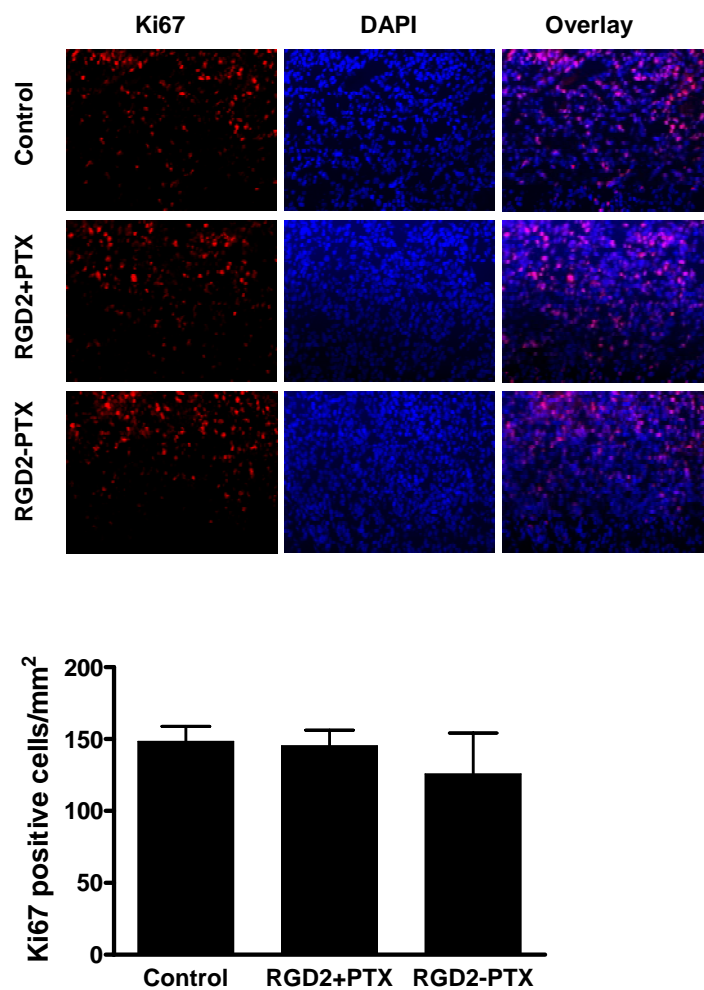
Fig. 9. (A) Immunofluorescence staining of Ki67, DAPI, and the overlay for MDA-MB-435 tumor tissues from the control, RGD2+PTX, and RGD2-PTX treatment groups. (B) Ki67 positive cell counting showed little or no difference among three treatment groups (P > 0.05).

KEY RESEARCH ACCOMPLISHMENTS

- We have developed a series of new RGD peptide tracers for PET imaging of tumor integrin expression;
- We have demonstrated the feasibility of suitably labeled RGD peptide to quantify integrin receptor level in vivo;
- We have synthesized dimeric RGD peptide-paclitaxel conjugate (E[c(RGDyK)]$_2$-PTX) for integrin targeted delivery of chemotherapeutics;
- We have tested the treatment efficacy of E[c(RGDyK)]$_2$-PTX conjugate in orthotopic breast cancer model and showed better anti-cancer effect of RGD-paclitaxel than RGD + paclitaxel combination.

REPORTABLE OUTCOMES

Publications:

1. Cao Q, Li Z-B, Chen K, Wu Z, He L, Neamati N, **Chen X**. Evaluation of Biodistribution and Anti-tumor Effect of a Dimeric RGD Peptide-paclitaxel Conjugate in Mice with Breast Cancer. *Mol Cancer Ther* (under review).
2. Wang H, Chen K, Cai W, Li Z, He L, Kashefi A, **Chen X**. Integrin Targeted Imaging and Therapy with RGD4C-TNF Fusion Protein. *Mol Cancer Ther* (under review).
3. Li Z-B, Wu Z, Chen X. Click Chemistry for ^{18}F-Labeling of RGD Peptides. *Bioconjug Chem* (in press, 2007).
4. Cai W, **Chen X**. Multimodality Molecular Imaging of Tumor Angiogenesis. *J Nucl Med* (in press, 2007).

5. Wu Z, Li Z-B, Cai W, He L, Chin FT, Li F, **Chen X**. microPET Imaging of Tumor $\alpha_v\beta_3$ Integrin Expression Using ^{18}F-labeled PEGylated Tetrameric RGD Peptide (^{18}F-FPRGD4). *J Nucl Med* 2007;48:1536-1544.

6. Li Z-B, Cai W, Cao Q, Chen K, Wu Z, He L, **Chen X**. ^{64}Cu-Labeled Tetrameric and Octameric RGD Peptides for MicroPET Imaging of Tumor $\alpha_v\beta_3$ Integrin Expression. *J Nucl Med*, 2007;48:1162-1171.
7. Wu Z, Li Z-B, Cai W, Chin FT, Li F, **Chen X**. ^{18}F-labeled mini-PEG spacered RGD dimer (^{18}F-FPRGD2): synthesis and microPET imaging of $\alpha_v\beta_3$ integrin expression. *Eur J Nucl Med Mol Imaging* 2007 May 5; [Epub ahead of print].
8. Cao Q, Cai W, Li T, Yang Y, Chen K, Xing L, **Chen X**. Combined Integrin siRNA Therapy and Radiotherapy of Breast Cancer. *Biochem Biophys Res Commun*. 2006; 351:726-732.
9. Hsu AR, Veeravagu A, Cai W, Hou LC, Tse VCK, **Chen X**. Integrin $\alpha_v\beta_3$ antagonists for anti-angiogenic cancer treatment. *Recent Patents on Anti-Cancer Drug Discovery*. 2007;2:143-160.
10. Cai W, **Chen X**. Anti-Angiogenic Cancer Therapy Based on Integrin Antagonism. *Current Medicinal Chemistry-Anti-Cancer Agents (CMC-ACA)*. 2006;6:407-428.
11. Dayam R, Aiello F, Wu Y, Garofalo A, **Chen X**, Neamati N. Discovery of Small Molecule Integrin $\alpha v\beta 3$ Receptor Antagonists as Novel Anticancer Agents. *J Med Chem*. 2006;49:4526-4534.
12. Cai W, Zhang X, Wu Y, **Chen X**. A thiol-reactive ^{18}F-labeling agent, N-[2-(4-^{18}F-fluorobenzamido)ethyl]maleimide, and synthesis of RGD peptide-based tracer for PET imaging of $\alpha_v\beta_3$ integrin expression. *J Nucl Med*. 2006;47:1172-1180.
13. Cai W, Gambhir SS, **Chen X**. Multimodality Tumor Imaging Targeting Integrin $\alpha v\beta 3$ Biotechniques. 2005;39:S6-S17 (Review).
14. Wu Y, Zhang X, Xiong Z, Cheng Z, Fisher Dr, Liu S, Gambhir SS, **Chen X**. MicroPET Imaging of Glioma alpha(v)-Integrin Expression Using ^{64}Cu-Labeled Tetrameric RGD Peptide. *J Nucl Med*.2005;46:1707-1718.
15. Zhang X, Xiong Z, Wu Y, Tseng JR, Gambhir SS, **Chen X**. Quantitative PET Imaging of Tumor Integrin $\alpha_v\beta_3$ Expression with [^{18}F]FRGD2. *J Nucl Med*. 2006;47:113-121.

16. **Chen X**, Plasencia C, Hou Y, Neamati N. Synthesis and Biological Evaluation of Dimeric RGD Peptide-Paclitaxel Conjugate as Model for Integrin Targeted Drug Delivery. *J Med Chem* 2005;48:1098-1106.
17. **Chen X**, Tohme M, Park R, Hou Y, Bading JR, Conti PS. MicroPET Imaging of $\alpha_v\beta_3$ Integrin Expression with ^{18}F-Labeled Dimeric RGD Peptide. *Mol Imaging* 2004;3:96-104.

CONCLUSIONS

Integrin αvβ3 is a viable target for breast cancer imaging and therapy. The receptor affinity and adhesion ability of RGD peptides can be enhanced through polyvalency effect. Suitably labeled RGD peptides allow tumor delineation based on integrin expression. The ability of ^{18}F-labeled RGD peptide for quantification of integrin expression in a nono-invasive manner allow clinical translation of this class of compounds for cancer imaging and patient stratification based on integrin status.

The in vitro potency of RGD-paclitaxel is similar to paclitaxel, but the tumor accumulation of RGD-paclitaxel in vivo is significantly higher than paclitaxel, resulting in improved anti-cancer effect. Development of paclitaxel conjugates with further improved tumor specific cytotoxicity is currently in progress.

REFERENCES

None.

APPENDICES

None.